Transformation and sublimation of interstellar ices: insights from laboratory experiments and astronomical observations

Carvalho Santos, J. de

6. Formation of carbonyl sulfide (OCS) via SH radicals in interstellar CO-rich ice under dense cloud conditions

Carbonyl sulfide (OCS) is widely observed in the gas phase toward star-forming regions and was the first of the only two sulfur-bearing species to be detected in interstellar ices so far. However, the chemical network governing its formation is still not fully understood. While the sulfurization of CO and the oxidation of CS are often invoked to form OCS, other mechanisms could have a significant contribution. In particular, the multistep reaction involving CO and SH is a good candidate for forming a significant portion of the OCS in dense cloud environments. We aim to constrain the viability of the CO + SH route for forming solid OCS in the interstellar medium, in a similar manner as CO+OH is known to produce CO_2 ice. This is achieved by conducting a systematic laboratory investigation of the targeted reactions on interstellar ice analogs under dense cloud conditions. We used an ultrahigh vacuum chamber to simultaneously deposit CO, H_2S, and atomic H at 10 K. SH radicals produced in situ via hydrogen abstraction from H_2S reacted with CO to form OCS. We monitored the ice composition during deposition and subsequent warm-up by means of Fourier-transform reflection absorption infrared spectroscopy (RAIRS). Complementarily, desorbed species were recorded with a quadrupole mass spectrometer (QMS) during temperature-programmed desorption (TPD) experiments. Control experiments were performed to secure the product identification. We also explored the effect of different H_2S:CO mixing ratios—with decreasing H_2S concentrations—on the OCS formation yield. OCS is efficiently formed through surface reactions involving CO, H_2S, and H atoms. The suggested underlying mechanism behind OCS formation is CO + SH → HSCO, followed by HSCO + H → OCS + H_2. The OCS yield reduces slowly, but remains significant with increasing CO:H_2S mixing ratios (CO:H_2S = 1:1, 5:1, 10:1, and 20:1). Our experiments provide unambiguous evidence that OCS can be formed from CO + SH in the presence of H atoms. This route remains efficient for large H_2S dilutions (5% with respect to CO), suggesting that it is a viable mechanism in interstellar ices. Given that SH radicals can be created in clouds over a wide evolutionary timescale, this mechanism could make a non-negligible contribution to the formation of interstellar OCS ice.

J. C. Santos, H. Linnartz, K.-J. Chuang. 2024, Astronomy and Astrophysics, 690, A24.

6.1 Introduction

Among the over 300 molecules detected in the interstellar medium to date[1], those that contain sulfur constitute a particularly conspicuous chemical family. They are observed in the gas phase throughout a wide evolutionary time span, from clouds (e.g., Drdla *et al.* 1989; Navarro-Almaida *et al.* 2020; Spezzano *et al.* 2022; Esplugues *et al.* 2022) to protostars (e.g., Blake *et al.* 1987, 1994; van der Tak *et al.* 2003; Li *et al.* 2015; Drozdovskaya *et al.* 2018; Codella *et al.* 2021; Artur de la Villarmois *et al.* 2023; Fontani *et al.* 2023; Kushwahaa *et al.* 2023), protoplanetary disks (Fuente *et al.* 2010; Phuong *et al.* 2018; Semenov *et al.* 2018; Le Gal *et al.* 2019; Rivière-Marichalar *et al.* 2021; Le Gal *et al.* 2021; Booth *et al.* 2024), and Solar System bodies (Smith *et al.* 1980; Bockelée-Morvan *et al.* 2000a; Hibbitts *et al.* 2000; Jessup *et al.* 2007; Moullet *et al.* 2008, 2013; Cartwright *et al.* 2020; Biver *et al.* 2021a,b; Calmonte *et al.* 2016; Altwegg *et al.* 2022). The species detected so far range in size, from simple diatomic molecules such as CS and SO to the thiols CH_3SH and CH_3CH_2SH (Linke *et al.* 1979; Gibb *et al.* 2000; Cernicharo *et al.* 2012; Kolesniková *et al.* 2014; Zapata *et al.* 2015; Müller *et al.* 2016; Majumdar *et al.* 2016; Rodríguez-Almeida *et al.* 2021a).

As opposed to gas-phase observations, however, only two sulfurated molecules have been detected in interstellar ices to date: OCS and SO_2 (Palumbo *et al.* 1995; Boogert *et al.* 1997; Palumbo *et al.* 1997; Öberg *et al.* 2008; Boogert *et al.* 2022; McClure *et al.* 2023; Rocha *et al.* 2024). This is probably in large part due to their low abundances, combined with the intrinsic limitations of solid-state observations, such as the broadness of the features and their high degeneracy. Nonetheless, these confirmed ice species already bring vast chemical ramifications, as they can act as reactants to form more complex organosulfur compounds, some of which have key biochemical roles (see, e.g., McAnally *et al.* 2024). However, despite their astrochemical significance, many open questions remain regarding the formation pathways of these small sulfur-bearing molecules in the solid state.

One particularly important case is that of carbonyl sulfide (OCS), a major gaseous sulfur carrier commonly detected toward young stellar objects (e.g., van der Tak *et al.* 2003; Herpin *et al.* 2009; Oya *et al.* 2016; Drozdovskaya *et al.* 2018; Kushwahaa *et al.* 2023; López-Gallifa *et al.* 2024; Santos *et al.* 2024c). OCS is also frequently detected in interstellar ices (see, e.g., Palumbo *et al.* 1997; Boogert *et al.* 2022), in part facilitated by the characteristically large absorption band strength of its 4.9 μm feature in comparison to other ice species (e.g., $\sim 1.2\times10^{-16}$ cm molecule^{-1} as measured by Yarnall & Hudson 2022 for pure OCS ice at 10 K; See also Hudgins *et al.* 1993). Observed OCS abundances in both protostellar ices and hot-core gas point to a solid-state formation mechanism occurring predominately during the high-density pre-stellar core stage ($A_V > 9$, $n_H \gtrsim 10^5$ cm^{-3}) after the onset of the CO catastrophic freeze-out (Palumbo *et al.* 1997; Boogert *et al.* 2022; Santos *et al.* 2024c). This proposed icy origin of OCS is corroborated by gas-phase astrochemical models, which fail to reproduce observed OCS abundances (Loison *et al.* 2012). In the inner regions of the protostellar envelope, thermal heating by the protostar causes the volatile ice content to fully sublimate, enabling the bulk of the gaseous OCS observations.

So far, the two most commonly proposed routes to OCS involve either the oxidation of CS or the sulfurization of CO in the solid state (Palumbo *et al.* 1997; Ferrante *et al.* 2008; Adriaens *et al.* 2010; Chen *et al.* 2015; Laas & Caselli 2019; Shingledecker *et al.* 2020; Boogert *et al.* 2022):

$$\mathrm{CS + O \rightarrow OCS}, \tag{6.1}$$

$$\mathrm{CO + S \rightarrow OCS}. \tag{6.2}$$

[1] https://cdms.astro.uni-koeln.de/

However, CS abundances are considerably smaller ($\lesssim$ 2.5%) than those of OCS, casting doubts on the extent of the contribution from Reaction 6.1 to the interstellar OCS content (Boogert *et al.* 2022). Reaction 6.2 is more often invoked as the dominant route to OCS, especially due to the large availability of solid-state CO as a reactant in the post freeze-out stage.

Hydrogen in its atomic form is also abundant in pre-stellar cores (H/CO$\sim$1$-$10, Lacy *et al.* 1994; Goldsmith & Li 2005) and can trigger solid-state reactions of relevance to the sulfur network. Following adsorption onto dust grains, sulfur atoms are subject to successive hydrogenation reactions to form SH and H_2S via the steps:

$$S + H \rightarrow SH, \tag{6.3}$$

$$SH + H \rightarrow H_2S, \tag{6.4}$$

both of which are predicted by astrochemical models to proceed very efficiently (see, e.g., Garrod *et al.* 2007; Druard & Wakelam 2012; Esplugues *et al.* 2014; Vidal *et al.* 2017). Once H_2S ice is formed, it can further react with another hydrogen atom via an abstraction route (Lamberts & Kästner 2017; Oba *et al.* 2018, 2019; Santos *et al.* 2023b), or be dissociated through energetic processing (e.g., Jiménez-Escobar *et al.* 2014a; Chen *et al.* 2015; Cazaux *et al.* 2022):

$$H_2S + H \rightarrow SH + H_2, \tag{6.5a}$$

$$H_2S + h\nu \rightarrow SH + H, \tag{6.5b}$$

thus partially replenishing the SH ice content. As a result, SH radicals will likely be present in the ice throughout a wide evolutionary time span, and could potentially serve as an alternative source of sulfur in the formation of OCS.

A particularly promising pathway is the reaction between SH and CO followed by a hydrogen abstraction step (Adriaens *et al.* 2010; Chen *et al.* 2015):

$$SH + CO \rightarrow HSCO, \tag{6.6}$$

$$HSCO + H \rightarrow OCS + H_2, \tag{6.7}$$

which involves the formation of the intermediate complex HSCO. This pathway is analogous to the case of CO_2 ice formation from CO and OH through the HOCO complex (e.g., Oba *et al.* 2010b; Ioppolo *et al.* 2011; Noble *et al.* 2011; Qasim *et al.* 2019; Molpeceres *et al.* 2023). In the case of CO_2, Molpeceres *et al.* (2023) find that the spontaneous dissociation of HOCO into H and CO_2 is not energetically viable, and thus the formation of the latter is only possible through the interaction of the HOCO intermediate with a hydrogen atom. Similarly, HSCO is also prevented from spontaneously dissociating into OCS and H (Adriaens *et al.* 2010). In the laboratory, OCS is readily formed in energetically processed CO:H_2S ice mixtures (Ferrante *et al.* 2008; Garozzo *et al.* 2010; Jiménez-Escobar *et al.* 2014a; Chen *et al.* 2015), for which both reactions involving CO + S and CO + SH have been suggested as possible formation routes. Moreover, Nguyen *et al.* (2021b) allude to the possibility of forming OCS through reactions 6.6 and 6.7 in a CO:H_2S ice mixture exposed to hydrogen atoms, but without exploring this pathway further. Dedicated laboratory studies assessing this particular reaction pathway to OCS formation are therefore still highly warranted.

In the present experimental work, we investigate the viability of OCS formation via Reactions 6.6 and 6.7 under dark cloud conditions by simultaneously depositing H_2S, CO, and H atoms at 10 K. The SH radicals are produced via Reaction 6.5a, and are subsequently subject to reaction with neighboring species. The experimental methods used in this work are described in Sect. 6.2. In Sect. 6.3 we present and discuss our main results. Their astrophysical implications are elaborated in Sect. 6.4, followed by a summary of our main findings in Sect. 6.5.

6.2 Experimental methods

Table 6.1: Experiments performed in this work.

Experiment	Label	CO flux (cm^{-2} s^{-1})	H_2S flux (cm^{-2} s^{-1})	H flux (cm^{-2} s^{-1})	CO:H_2S:H
$CO + H_2S + H$	1	1.8×10^{11}	1.8×10^{11}	5.5×10^{12}	1:1:30
$CO + H_2S$	2	1.8×10^{11}	1.8×10^{11}	–	1:1:0
$^{13}C^{18}O + H_2S + H$	3	1.8×10^{11}	1.8×10^{11}	5.5×10^{12}	1:1:30
$CO + H_2S + H$	4	9.3×10^{11}	1.8×10^{11}	5.5×10^{12}	5:1:30
$CO + H_2S + H$	5	1.8×10^{12}	1.8×10^{11}	5.5×10^{12}	10:1:30
$CO + H_2S + H$	6	3.7×10^{12}	1.8×10^{11}	5.5×10^{12}	20:1:30

This work uses the ultrahigh vacuum (UHV) setup SURFRESIDE[3], for which detailed descriptions are provided elsewhere (Ioppolo *et al.* 2013; Qasim *et al.* 2020b). Briefly, this setup contains a main chamber that operates at base pressures of $\sim 5 \times 10^{-10}$ mbar, and at the center of which a gold-plated copper substrate is mounted on the tip of a closed-cycle helium cryostat. Resistive heaters are used to vary the substrate temperature between 8 and 450 K, as monitored by two silicon diode sensors with a relative accuracy of 0.5 K. A hydrogen atom beam source (HABS Tschersich 2000) generates H atoms that are subsequently cooled down by colliding with a nose-shaped quartz pipe before reaching the substrate. As H atoms are injected into the chamber, gases of H_2S (Linde, 99.5% purity) and CO (Linde, 99.997% purity) are concomitantly admitted through two separate all-metal leak valves. The heavier isotopolog $^{13}C^{18}O$ (Sigma-Aldrich, 95% purity ^{18}O, 99% purity ^{13}C) is also used to assist in the product identification. Fourier-transform reflection-absorption infrared spectroscopy (FT-RAIRS) is used to monitor ice growth in the range of 700 to 4000 cm^{-1} with 1 cm^{-1} spectral resolution. When the deposition is complete, temperature-programmed desorption (TPD) experiments are performed by heating the sample at a constant rate of 5 K min^{-1}. During TPD, the solid phase is monitored by RAIRS, while the sublimated species are immediately ionized by 70 eV electron impact and are recorded by a quadrupole mass spectrometer (QMS). The variation of the substrate temperature during the collection of each IR TPD spectrum is of ∼10 K.

The absolute abundance of the ice species can be derived from their integrated infrared absorbance ($\int Abs(\nu)d\nu$) using a modified Beer-Lambert law:

$$N_X = \ln 10 \frac{\int Abs(\nu)d\nu}{A'(X)}, \tag{6.8}$$

where N_X is the column density in molecules cm^{-2} and $A'(X)$ is the apparent absorption band strength in cm $molecule^{-1}$ of a given species. We use $A'(CO)_{\sim 2142 cm^{-1}} \sim (4.2 \pm 0.3) \times 10^{-17}$ cm $molecule^{-1}$ and $A'(H_2S)_{\sim 2553 cm^{-1}} \sim (4.7 \pm 0.1) \times 10^{-17}$ cm $molecule^{-1}$, as measured for our reflection-mode IR settings using the laser-interference technique (see Santos *et al.* 2023b for the case of H_2S). For the target product, OCS, we employ the band strength of $A'(OCS)_{\sim 2043 cm^{-1}} \sim (1.2 \pm 0.1) \times 10^{-16}$ cm $molecule^{-1}$ measured in transmission mode by Yarnall & Hudson (2022), and correct it by an averaged transmission-to-reflection conversion factor of 3.2 derived with our experimental setup (see Santos *et al.* 2023b for the case of H_2S, which was later combined with CO ice depositions to derive the averaged setup-specific conversion factor).

Table 6.1 summarizes the experiments performed in this work. All depositions are carried out for 180 minutes with a constant substrate temperature of 10 K. The relative errors of

the H-atom flux, as well as both molecule fluxes, are estimated to be $\lesssim 5\%$. The latter are estimated from evaluating the ice growth rate in multiple pure-ice deposition experiments. To estimate the former, multiple experiments to calibrate the relative H-atom flux are conducted. These consist of trapping H atoms inside O_2 ice matrices and monitoring the formation of HO_2, which is proportional to the H-atom flux provided that O_2 is overabundant relative to H (Ioppolo *et al.* 2013; Fedoseev *et al.* 2015b). The instrumental uncertainties in the integrated QMS and IR signals are derived from the corresponding integrated spectral noise for the same band width.

6.3 Results and discussion

6.3.1 OCS formation

Panel (a) of Fig. 6.1 shows the infrared spectra obtained after codeposition of CO, H_2S, and H atoms (1:1:30, experiment 1) at 10 K, as well as after a control experiment of only CO and H_2S (1:1, experiment 2). When CO and H_2S are exposed to hydrogen atoms, a new feature appears at $\sim$ 2043 cm^{-1} ($\sim$4.89 μm) with a full-width at half maximum (FWHM) of $\sim$15 cm^{-1} ($\sim$0.03 μm). Based on its peak position and the ice elemental composition (i.e., C, O, S, and H), this feature is assigned as the CO-stretching mode of OCS (ν_1, Yarnall & Hudson 2022)[2]. The band's FWHM and peak position are also consistent with previously reported values for OCS in CO-rich ices measured in reflection mode (Ferrante *et al.* 2008). To confirm this assignment, an analogous experiment is performed with a heavier isotopolog of carbon monoxide, $^{13}C^{18}O$ (experiment 3: blue spectrum in Fig. 6.1). In this case, the $^{18}O^{13}CS$ ν_1 feature appears at $\sim$ 1954 cm^{-1} ($\sim$5.12 μm) in accordance with the expected redshift of the heavier isotopolog. During TPD, both features at $\sim$ 2043 cm^{-1} and $\sim$ 1954 cm^{-1} disappear from the ice in the same temperature interval of $70 - 100$ K (Panels b) and c) in Fig. 6.1), thus signaling that the two bands correspond to the same molecule.

Complementarily to the infrared spectra, data obtained by the QMS during TPD can also be used to strengthen the OCS identification. Panel (a) of Fig. 6.2 displays the signal for m/z = 60 recorded during the warm-up of the ice sample in the CO + H_2S + H experiment. This mass-to-charge ratio corresponds to the molecular ion of OCS, its strongest signal resulting from 70 eV electron impact as listed in NIST[3]. A desorption feature appears peaking at $\sim$89 K, in agreement with previously reported desorption temperatures of OCS (Ferrante *et al.* 2008; Nguyen *et al.* 2021b). In the isotope-labeled experiment, a similar desorption peak is observed for m/z = 63, consistent with the mass shift corresponding to the molecular ion of $^{18}O^{13}CS$. Moreover, no peak signal is detected for m/z = 60, indicating that this same feature appearing in experiment 1 corresponds uniquely to carbonyl sulfide. The desorption temperature of OCS as measured by the QMS correlates with the disappearance of the $\sim$ 2043 cm^{-1} feature in the infrared spectra taken during TPD, as indicated by the area of this infrared band as a function of substrate temperature (Fig. 6.2 panel b). Both the infrared and QMS data therefore provide unequivocal evidence for the formation of OCS as a result of interactions between H_2S, CO, and H atoms in the solid state.

Aside from OCS, another S-bearing species that could presumably be formed under our experimental conditions is thioformic acid, HCOSH. Indeed, formation routes via either the hydrogenation of the HSCO intermediate or the interaction between HCO + SH have been proposed by Rodríguez-Almeida *et al.* (2021a) to explain HCOSH observations toward the giant molecular cloud G+0.693–0.027, with the former subsequently verified theoretically by Molpeceres *et al.* (2021). Although HCOSH has been shown to form upon keV electron

[2]The numbers assigned to the CS and CO stretches of OCS are interchangeable. In this work, we adopt the notation from Yarnall & Hudson (2022).

[3]https://webbook.nist.gov/chemistry/

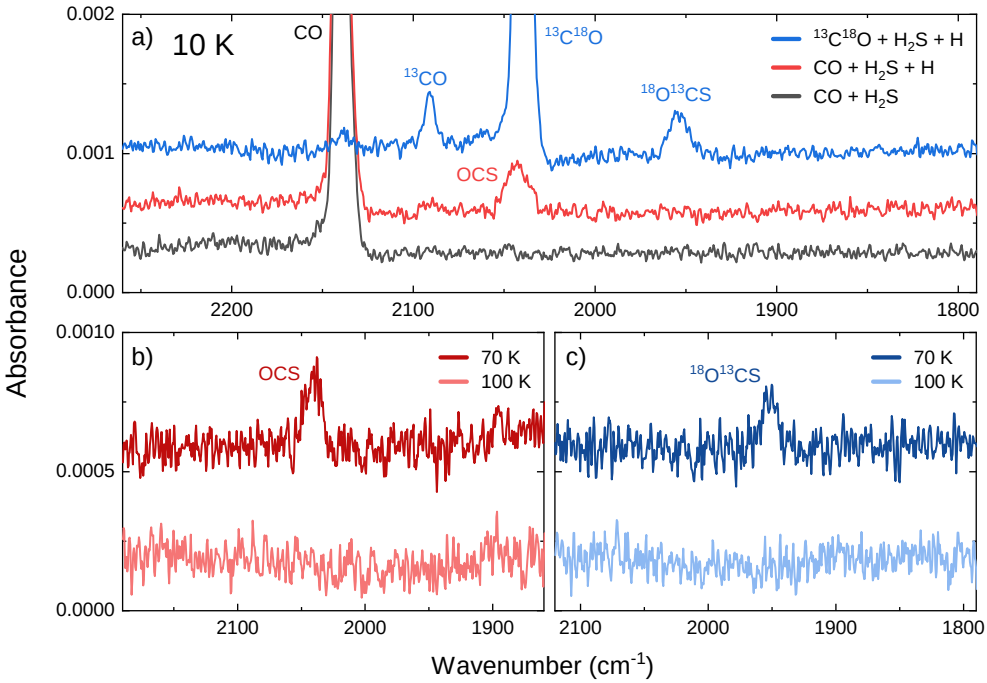

Figure 6.1: Infrared data confirming the formation of OCS from CO, H_2S, and H atoms. Panel (a): Spectrum collected after deposition of CO + H_2S + H (experiment 1, red) together with the control experiment without H atoms (experiment 2, gray) and the isotope-labeled experiment with $^{13}C^{18}O$ (experiment 3, blue). Small features assigned to ^{13}CO and ^{12}CO are due to minor contaminations from the gas bottle (respectively, $\sim$ 4% and $\sim$ 2% with respect to $^{13}C^{18}O$). Panel (b): Infrared spectra acquired during TPD following the deposition of experiment 1. The spectrum in dark red (upper) is taken at $\sim$70 K, and the one in light red (lower) is taken at $\sim$100 K. Panel (c): Same as panel (b), but for the isotope-labeled experiment. In all panels, only the relevant frequency range is shown and the spectra are offset for clarity.

irradiation of H_2S:CO ices (Wang *et al.* 2022), Nguyen *et al.* (2021b) only tentatively identify this product in similar hydrogenation experiments on H_2S:CO ices. No evidence for this species is observed in our experiments above the instrumental detection limit. Likewise, we do not detect any signal of volatile sulfur allotropes such as S_2 or S_3, nor of hydrogenated sulfur chains such as H_2S_2 or H_2S_3—which could presumably be formed from the association of sulfur atoms produced via hydrogen abstraction reactions from SH radicals. This leads to the conclusion that the potential production of the atomic S does not proceed efficiently under our experimental conditions. Moreover, as no H_2S_2 is detected, the recombination of two SH radicals is also likely not efficient in the present experiments—signaling that HS radicals are efficiently consumed, both by reacting with CO leading to OCS and by reacting with H to reform H_2S.

Reactions 6.6 and 6.7 are therefore the predominant contributors to the formation of OCS in our experiments. As shown by Nguyen *et al.* (2021b), however, the backward reactions are also viable. Once formed, OCS can be hydrogenated into the complex intermediate HSCO, which in turn can further react with another H atom to yield CO and H_2S, as well as dissociate back into the reactants SH and CO (Adriaens *et al.* 2010; Nguyen *et al.* 2021b; Molpeceres *et al.* 2021). The effective amount of OCS detected will therefore be subject to these two

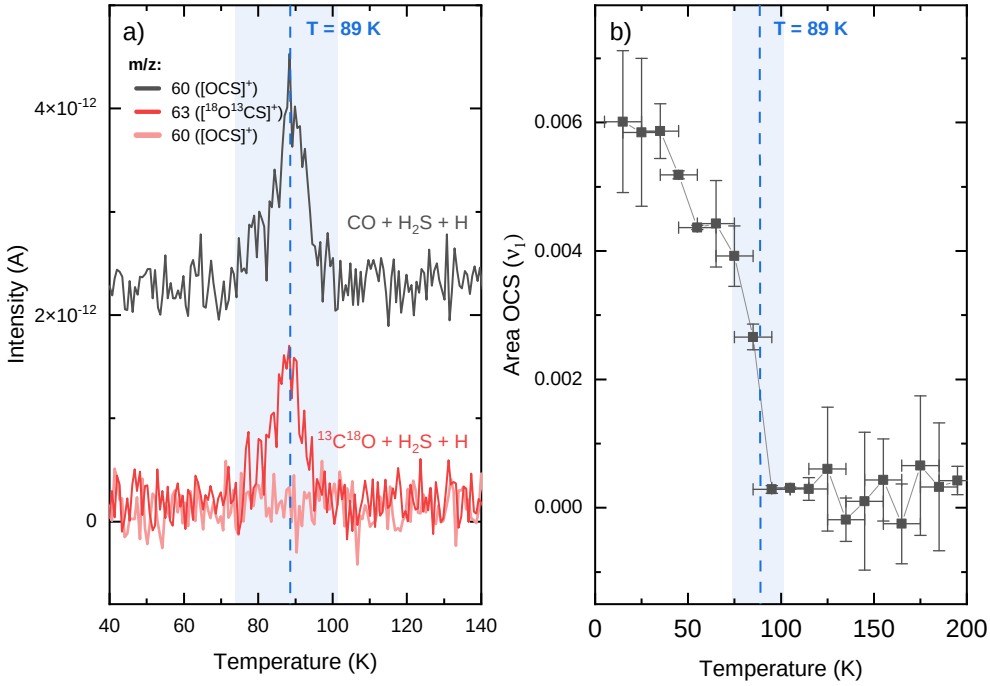

Figure 6.2: Complementary QMS and infrared data acquired during TPD confirming the OCS detection. Panel (a): TPD-QMS signal recorded for m/z = 60 after the deposition of CO + H_2S + H (experiment 1, gray), as well as those for m/z = 63 (dark red) and m/z = 60 (light red) after the deposition of $^{13}C^{18}O + H_2S + H$ (experiment 3). The blue shadowed region denotes the range of desorption, and the dashed line highlights the peak desorption temperature. Signals from different experiments are offset for clarity. Panel (b): Area of the OCS ν_1 band as a function of temperature during TPD following the deposition of experiment 1. The uncertainties in the horizontal axis are due to the substrate temperature variation of ∼10 K during the collection of each IR TPD spectrum. The blue shadowed area and dashed line are reproductions of the range and peak position shown in Panel (a).

competing directions.

6.3.2 Effects of larger CO fractions

Once the possibility of forming OCS from CO and SH is ascertained, the next question to arise is that regarding the viability of this route in more astronomically representative ice mixing ratios. To date, there are no convincing detections of H_2S in interstellar ices, with upper limits estimated to be ≤0.7% with respect to water (Jiménez-Escobar & Muñoz Caro 2011b). This would translate to ice abundance upper limits of roughly a few percent with respect to CO (e.g., $N(H_2S)/N(CO) \lesssim 0.035$ if assuming $N(CO)/N(H_2O) \sim 0.21$ according to the median CO ice abundance value with respect to H_2O derived for low-mass young stellar objects (LYSOs) in Boogert *et al.* 2015). Accordingly, we performed similar depositions with larger fractions of CO with respect to H_2S in order to assess how the dilution of the latter affects the yields of OCS. The deposition fluxes of H_2S and atomic H are kept the same in all experiments, with only variations in the CO flux (see Table 6.1). Figure 6.3 compares the relative intensities of the OCS signals obtained from both the IR and QMS data for the

different mixing ratios explored here (i.e., CO:H_2S = 1:1, 5:1, 10:1, and 20:1). The areas of the OCS ν_1 vibrational modes for each mixing ratio after deposition are normalized to that of experiment 1, which yielded the largest absolute amount of products. Similarly, the areas of the m/z = 60 desorption band at $\sim$ 89 K are also normalized to that of experiment 1.

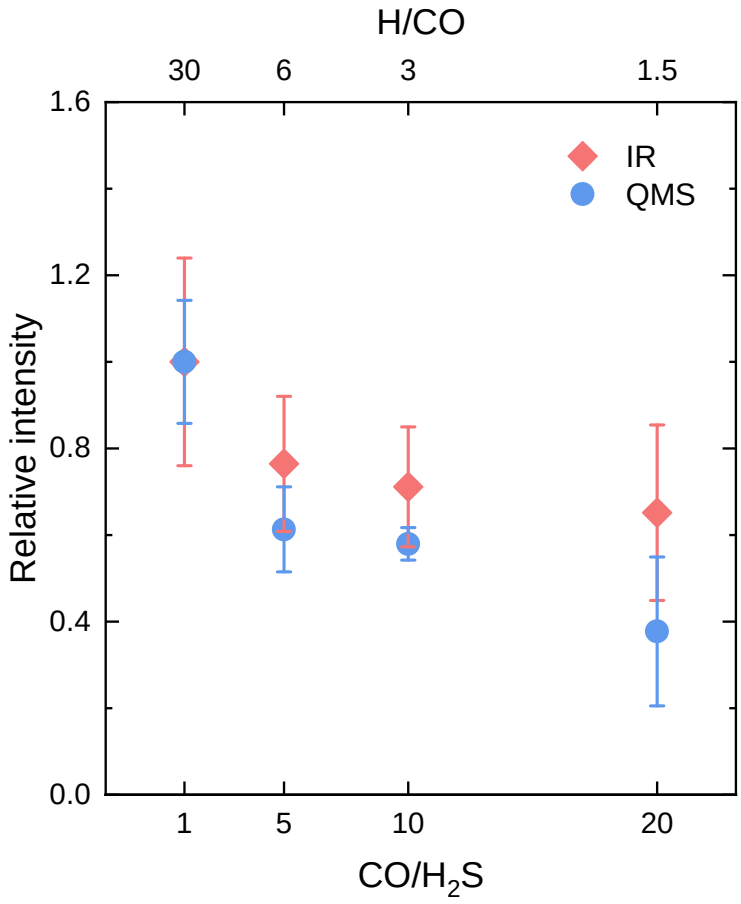

Figure 6.3: Integrated intensities of the infrared and QMS features of OCS for different flux conditions: CO:H_2S = 1:1, 5:1, 10:1, and 20:1. The infrared value is derived from the area of the ν_1 mode of OCS, while the QMS counterpart is calculated from the integrated desorption band for m/z = 60 peaking at $\sim$89 K. The resulting yields are normalized to that of experiment 1 (CO:H_2S = 1:1). The upper x-axis shows the corresponding ratios of H/CO, signaling the decrease in H-atom availability with increasing CO fractions.

Overall, the infrared and QMS data provide consistent OCS yields within their respective error bars, and signal that dilution of H_2S in CO reduces but does not impede OCS formation under our experimental conditions. Indeed, in the highest dilution case (5% H_2S with respect to CO), OCS production diminishes by $\sim$ 50% (the mean value between the infrared and QMS results) in comparison to the nondiluted reference experiment (100% H_2S with respect to CO). This decrease in OCS yield is likely governed by the reduced number of available H atoms in experiments with larger CO fractions, as opposed to a diminishing effectiveness of the OCS formation. As well established by previous works, the interaction of CO with H atoms in the solid state initiates a chain of reactions leading to H_2CO and CH_3OH (Tielens &

Hagen 1982; Charnley *et al.* 1992; Hiraoka *et al.* 1994; Watanabe & Kouchi 2002; Fuchs *et al.* 2009; Santos *et al.* 2022b), which efficiently consumes the available atomic hydrogen in the system. Increasing the CO deposition flux while maintaining a fixed H-atom flux therefore results in less hydrogen being able to react with other species. This decrease in available H atoms will have a greater impact on the formation of SH radicals (Reaction 6.5a) than on the final abstraction step (Reaction 6.7), as the latter is predicted to be barrierless (Adriaens *et al.* 2010), whereas the former requires quantum tunneling through a barrier of ∼1500 K (Lamberts & Kästner 2017). The slowly decreasing trend in Fig. 6.3 suggests that OCS can still be formed at 10 K in ice mixtures with CO:H_2S of higher than 20:1 and H:CO of as low as 1.5:1. The formation of OCS from CO + SH could therefore make a non-negligible contribution to the observed OCS in interstellar ices, as discussed below.

6.4 Astrophysical implications

The reaction network probed in this work is shown in Fig. 6.4. Aside from OCS, other closed-shell species also formed within this network are H_2S_2 (Santos *et al.* 2023b), H_2CO, and CH_3OH (Tielens & Hagen 1982; Charnley *et al.* 1992; Hiraoka *et al.* 1994; Watanabe & Kouchi 2002; Fuchs *et al.* 2009; Santos *et al.* 2022b). In our experiments, H_2S is used as a source of SH radicals via a hydrogen abstraction (Reaction 6.5a) to avoid reactions with S atoms to interfere with the analysis. In the ISM, however, SH will not only be produced from H_2S but also from the hydrogenation of sulfur atoms that adsorb onto dust grains (Reaction 6.3). Observations of singly and doubly deuterated H_2S in Class 0 sources suggest that the bulk of its formation takes place early in the evolution of a cloud, before the catastrophic CO freeze-out stage begins (Ceccarelli *et al.* 2014). Accordingly, SH radicals will be available in the ice as early as during the low-density prestellar core stage. As the cloud evolves and the density of the environment increases, most of the available S atoms will be converted into H_2S. Nonetheless, SH radicals can still be formed through Reaction 6.5a or through dissociation reactions induced by energetic processing. As a result, SH will remain a viable reactant throughout a large fraction of a cloud's lifetime.

Observations of OCS toward massive young stellar objects (MYSOs) reveal that its 4.9 μm feature is best fitted by reference spectra of OCS in a CH_3OH-rich environment (Palumbo *et al.* 1997; Boogert *et al.* 2022). Their column density ratios (N(OCS)/N(CH_3OH)) in both ice and gas have similarly narrow distributions and comparable median values (within a factor of 3, Santos *et al.* 2024c), strengthening the hypothesis that both coexist in similar ice environments. Moreover, observed ice abundances of OCS and CH_3OH are correlated (Boogert *et al.* 2022), suggesting a strong chemical link between the two molecules. As methanol is known to be formed via the hydrogenation of CO in the solid phase, such observations are in line with CO being a common precursor between the two. This would imply that the bulk of OCS ice likely originates deep into dense clouds, in a dense environment post catastrophic CO freeze-out. Conversely, a large portion of the free sulfur atoms will likely be readily converted into H_2S at such densities. The reaction route proposed here could partially circumvent this issue, as SH radicals can be efficiently produced through a top-down mechanism (Reaction 6.5a). Moreover, estimated H_2S upper limits in ices are larger than the detected OCS abundances (Palumbo *et al.* 1997; Jiménez-Escobar & Muñoz Caro 2011b; Boogert *et al.* 2022), and thus this route remains viable in light of the observational evidence available so far. Overall, both CO + S and CO + SH routes likely contribute to the observed OCS abundances in interstellar ices, and exploration of the extent of this contribution warrants dedicated chemical modeling.

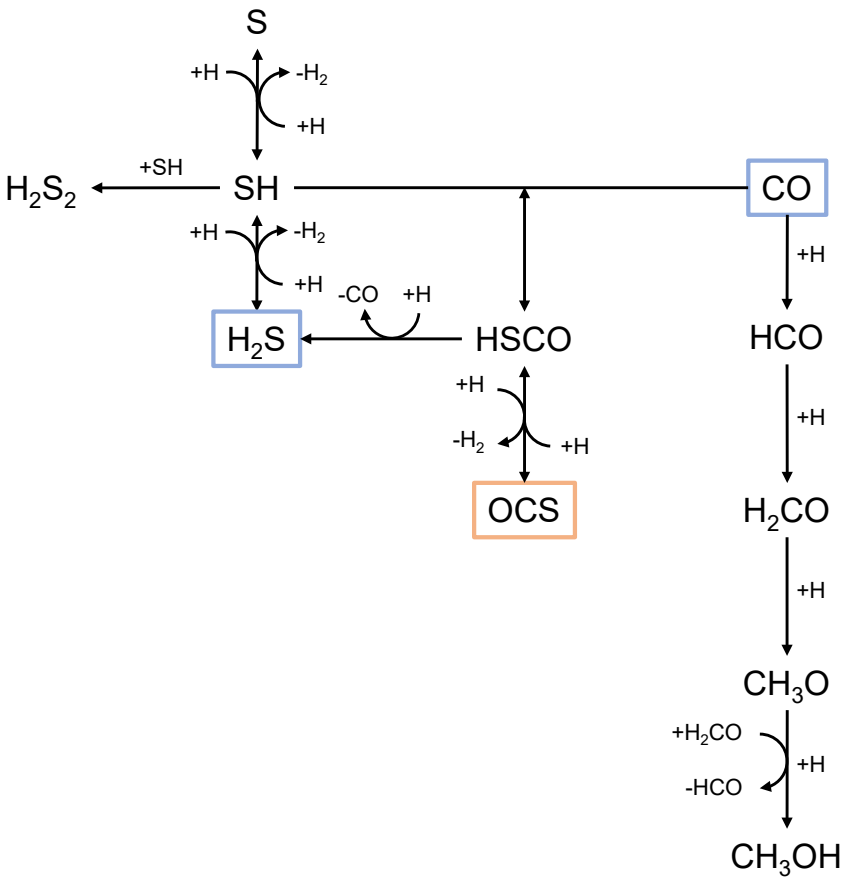

Figure 6.4: Reaction scheme proposed in this work. Blue boxes denote the deposited molecules and the orange box highlights the studied product, OCS. Hydrogen abstraction reactions from CH_3OH, H_2CO, and associated radicals are omitted for the sake of simplicity.

6.5 Conclusions

In this work, we conduct a systematic experimental investigation of the viability of forming OCS under dark cloud conditions from ice mixtures of CO, H_2S, and H atoms. Our main findings are summarized below:

- OCS can be efficiently formed at 10 K from solid-state reactions involving CO, H_2S, and H. The proposed underlying mechanism is via CO + SH $\rightarrow$ HSCO followed by HSCO + H $\rightarrow$ OCS + H_2, analogously to CO_2 ice.
- The OCS product yield decreases slowly with increasing initial CO/H_2S ratios and decreasing H-atom availability, resulting in $\sim$ 50% less OCS formation for a 20 times higher CO abundance relative to H_2S and fixed H-atom fluxes. This trend suggests that OCS can be efficiently formed via the proposed route in more representative interstellar ices, where H_2S is likely highly diluted in CO.
- SH can be produced both through bottom-up (S + H $\rightarrow$ SH) and top-down (H_2S + H $\rightarrow$

SH + H_2) routes, thus making it a favorable reactant to form OCS during the high-density, post-CO-freeze-out stage of prestellar cores. This is in line with both ice and gas-phase observations of OCS in protostars.

These findings suggest that the CO + SH reaction is potentially responsible for a non-negligible share of the interstellar OCS ice and therefore could be a valuable new addition to gas-grain chemical models focusing on sulfur species. In turn, such models could help to disentangle the contributions of the CO + SH and CO + S routes to forming OCS.

6.6 Acknowledgements

This work has been supported by the Danish National Research Foundation through the Center of Excellence "InterCat" (Grant agreement no.: DNRF150); the Netherlands Research School for Astronomy (NOVA); and the Dutch Astrochemistry Network II (DANII). KJC is grateful for support from NWO via a VENI fellowship (VI.Veni.212.296).